Numerical Modeling and Experimental Investigation of Biomedical Elastographic Problem by Using Plane Strain State Model

Michael Rychagov [1], Walaa Khaled [2], Stefan Reichling [2], Otto Bruhns [2], and Helmut Ermert [2]

[1] *Moscow Institute of Electronic Technology, Moscow, Russia; Email: mrychagov@miee.ru*

[2] *Ruhr-University Bochum, Bochum, Germany; Email: Walaa.Khaled@ruhr-uni-bochum.de*

Introduction

Ultrasonic elastographic imaging technique has been developed during last 10 years as a powerful method to image the elastic properties of soft biological tissues. The method consists of applying a small external, quasi-static compressions to the region of interest and use the set of radio frequency A-scans recorded before and after compression to estimate corresponding matrix of axial displacements by means of correlation technique. Afterwards, the displacement matrix is used to estimate the strain field, which can be interpreted as a relative measure of elasticity distribution and can be visualized as a gray scale elastogram. The main intention of our research was to consider the problem of visualization and reconstruction of tissue elastic properties within the framework of an appropriate inverse problem solution as well as its experimental exploration.

Approaches to the elastographic imaging

Presently, there are several approaches to mapping and representation of mechanical attributes of the constitutive tissues for the purposes of medical diagnostic information, i.e., *sonoelasticity imaging, elastography* and *inverse problem treatment* of strain images [1, 2].

The first approach involves the application of the low-frequency vibration energy to the tissue under the investigation and subsequent displaying the elastic modulus calculated from the local wavelength of the shear-wave, or the amplitude of the vibration that is related to the shear modulus [3 - 7].

Another approach, i.e., *elastography*, is aimed at the imaging of the local responses of the medium to an applied load by imaging the longitudinal or shear strain components produced by this load at different locations of the tissue. The load is applied to the tissue stepwise and resultant image is known as an *elastogram* [8 - 10].

The inverse problem approach is corresponded to the reconstruction of the elastic modulus from the displacement or the strain data obtained through elastography [11 - 17].

Depending on the *mechanical attributes* to be imaged, the above-mentioned approaches can be classified into two groups. *In the first group*, the imaged mechanical attributes are based on a direct estimation of one or more parameters from experimental observations. For example, in the case of elastography, the parameters to be imaged are the longitudinal strains, the shear strains or the Poisson's ratio estimated from the pre- and post-compression rf-data forming pre- and post-compression B-images. *In the second group*, the mechanical attribute to be imaged is based on an indirect estimation of one or many parameters obtained through the solution of an inverse problem using directly estimated data and a mechanical forward model of the tissue.

Adiabatic values of mechanical variables

It is well known, that the acoustic expansions are more nearly adiabatic than isothermal, so the sound speed as well as elastic characteristics of the medium have to be expressed in the limit of zero thermal conditions, i.e., when the compression is purely adiabatic. The final expressions for the connection between adiabatic and isothermal bulk modules of elasticity, K_S and K_T correspondingly, as well as between adiabatic and isothermal compressibilities, i.e., κ_S and κ_T, are following

$$\frac{1}{K_S} = \frac{1}{K_T} - \frac{T\beta^2}{C_p}, \quad \kappa_S = \kappa_T - \frac{T\beta^2}{C_p}, \tag{1}$$

where T is a temperature, β is a coefficient of the thermal expansion defining the fractional change in volume (or density) with temperature at constant pressure, C_P is a heat capacity at constant pressure [18].

For the adiabatic Young's modulus E_S and Poisson's ratio ν_S the following equations have to be used

$$E_S = \frac{E}{1 - ET\beta^2/9C_P}, \quad \nu_S = \frac{\nu + ET\beta^2/9C_P}{1 - ET\beta^2/9C_P}, \tag{2}$$

or, taking into account that in real conditions the value $ET\beta^2/C_P$ is negligibly small:

$$E_S = E + E^2\frac{T\beta^2}{9C_P}, \quad \nu_S = (1+\nu)E\frac{T\beta^2}{9C_P}. \tag{3}$$

Poisson's ratio for soft tissues

As it follows from the theory of elasticity [18], the values of Poisson's ratio have to be changed in the region from – ½ to ½. In fact, the values of Poisson's ratio are changed from 0 to ½ because there are no data on the materials which could have the values of $\nu_S < 0$, i.e., which could became thicker after the longitudinal elongation. Nevertheless, a supposition about the implicit incompressibility of the biological tissues leads to the instability in all basic equations describing the propagation of acoustic waves in continuous media.

The elastography is based on the principle that both deformations and strains in the tissues are very small (on the order of 1% or less) and the constitutive equations are considered to be linear. If the material is also assumed to be homogeneous, isotropic and viscoelastic, the longitudinal sound speed c_l and shear sound speed c_t for plane wave excitation can be expressed as

$$c_l = \left[\frac{E_S\,(1-\nu_S)}{\rho(1+\nu_S)\,(1-2\nu_S)}\right]^{1/2}, \tag{4.a}$$

$$c_t = \left[\frac{E_S}{2\rho(1+\nu_S)}\right]^{1/2}, \tag{4.b}$$

and appropriate wave equations have the form:

$$\frac{\partial^2 u_x}{\partial x^2} - \frac{1}{c_l^2}\frac{\partial^2 u_x}{\partial t^2} = 0\,, \quad \frac{\partial^2 u_y}{\partial x^2} - \frac{1}{c_t^2}\frac{\partial^2 u_y}{\partial t^2} = 0\,,$$

$$\frac{\partial^2 u_z}{\partial x^2} - \frac{1}{c_t^2}\frac{\partial^2 u_z}{\partial t^2} = 0\,. \qquad (5)$$

As it follows from Eq. (4), the shear sound speed c_t is much lower as the longitudinal one c_l. Theoretically, an inequality $c_l > \sqrt{2}c_t$ is taken place.

For biological tissues, an order-of-magnitude range for c_t of between 9 m/s and 100 m/s was given for a range of tissues including red blood cells, liver, kidney and muscle measured at 2.0, 6.5 and 14 MHz [19].

Combining two expressions in Eq. (4), we have

$$\nu_S = \frac{1}{2}\frac{c_l^2 - 2c_t^2}{c_l^2 - c_t^2}\,. \qquad (6)$$

The ranges of Poisson's ratio is thus predicted to be approximately from 0.497910 to 0.499 985 with reference longitudinal sound speed $c_l = 1550$ m/s.

Let us also estimate the values of ν_S using the approximation $\nu_S = 0.5 - \tilde{\nu}_S$ where $\tilde{\nu}_S$ is a characteristic value of the Poisson's ratio for biological tissue. From Eq. (4.a) we have

$$\tilde{\nu}_S = \frac{E_S}{2(3c_l^2\rho - E_S)}\,. \qquad (7)$$

By the derivation of Eq. (7), the values of $\tilde{\nu}_S^2$ were neglected. If the tissue elastic modulus in the normal breast fat will be used for an approximation, then having the value $E_S = 19 \pm 7$ kPa at 1 Hz loading frequency [20] and c_l=1476 m/s , ρ=928 kg /m^3, we obtain $\tilde{\nu}_S$=0.0000156639, and, correspondingly, ν_S=0.4999843361.

Numerical modeling of the elastographic problem

The simulation procedure for effective modeling of the elastographic problem contains three composite, and interactive parts, i. e., mechanical tool having in output the axial/lateral displacement at each of its nodes after the application of the external compression on the specimen; acoustical tool measuring the acoustic RF-signals and images inside the phantom before and after compression; and image formation technique (at the initial stage, the cross-correlation one) giving the estimations of the displacement field and strain distribution.

Fig. 1: Block-diagram of the integrated software for numerical modeling of elastographic problem

Forward elastographic modeling using plane strain state model

The numerical simulations were performed with MSC.Marc, a standard finite element program. To simulate the mechanical behavior of the tissue-mimicking phantoms, a two-dimensional mesh consisting of 2236 eight-node, isoparametric, arbitrary quadrilateral elements, written for incompressible or nearly incompressible plane strain applications, was used. In order to reproduce the experimental setup, the boundary conditions shown in Fig. 2 were applied to the model.

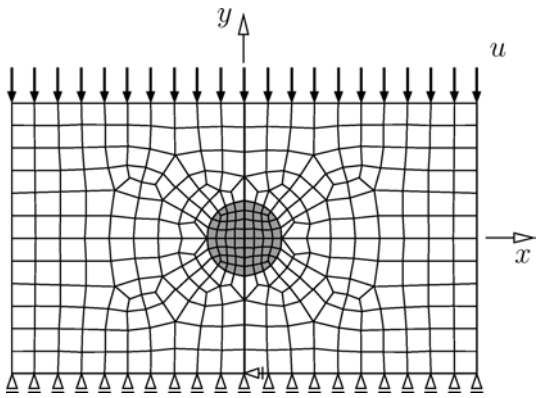

Fig. 2: Sketch of the the finite element discretization with applied boundary conditions

All nodes on the upper and lower boundary can move freely in x-direction, whereas the movement in y-direction is prescribed. In all FE-analyses, the Young's modulus of the matrix was fixed at 32 kPa, while the Youngs's modulus of the inclusion was varied between 8 kPa and 160 kPa. The Poisson's ratio of both parts was set to 0.495. The appropriate results are given in Fig. 3.

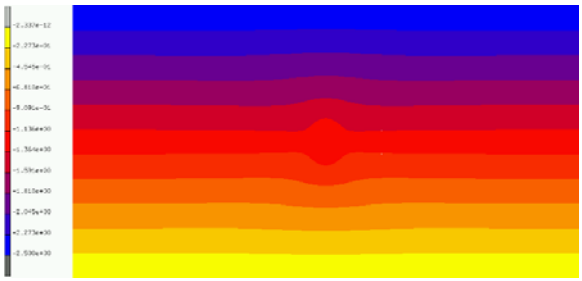

(a)

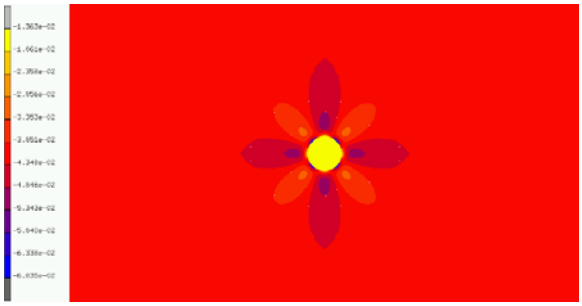

(b)

Fig. 3: Results of finite element analyses: displacement in y-direction (a) and strain ε_{yy} at E_{inc}/E_{mat}= 5 / 1 (b)

Results of experimental elastographic imaging for one-inclusion specimen

All experiments (Fig. 4) were performed using a commercially available ultrasound system SONOLINE Omnia (Siemens AG) equipped by a 7.5 MHz linear probe and sampled by a conventional gauge card on a desktop PC. A set of tissue-mimicking phantoms using different gelatin and agar concentrations were produced.

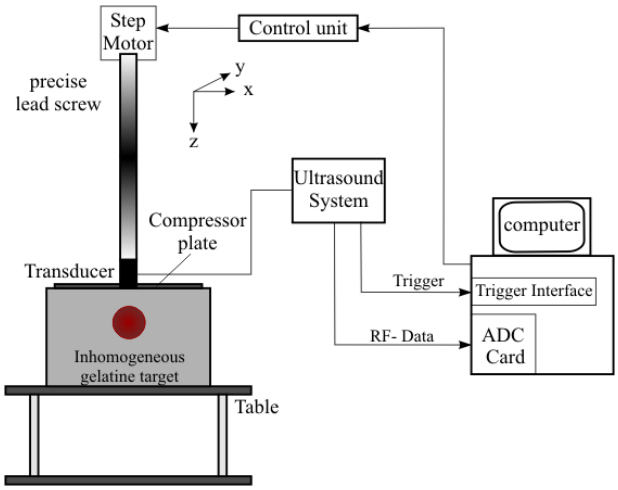

Fig. 4. Schematic diagram of the experimental setup

The strain images were collected by comparing echo signal sets obtained prior to and immediately after following less than 5% compression at the supposition that tissue properties are approximately linear and elastic.

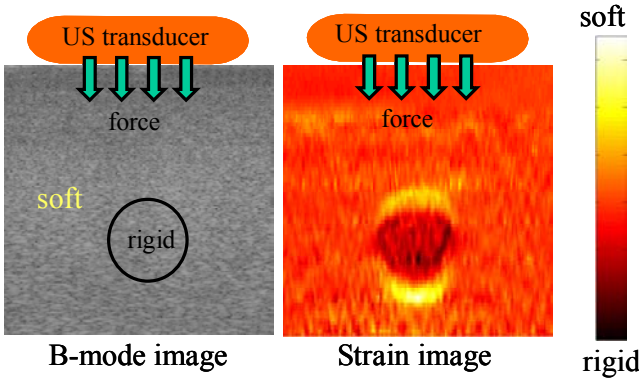

Fig. 5. *B*-mode imaging and elastographic one

Using the exact measurement of temporal displacements between two signal sets is the key to estimate strain. A phase root-seeking algorithm [21] has been utilized for fast and accurate displacement shift estimation, improving the accuracy and reducing the time needed for calculation.

In an experiment a tissue-like soft gelatin phantom with a hard agar inclusion (Ea/Eg = 5/1) is slightly compressed using the US transducer. The rigid body with cylinder shape in the phantom is not visible in the conventional B-mode image (Fig. 5, left). The same body can be clearly seen in the elastogram (strain image) to the right. Experimentally obtained images of displacement distribution and strain are given also in Fig. 6.

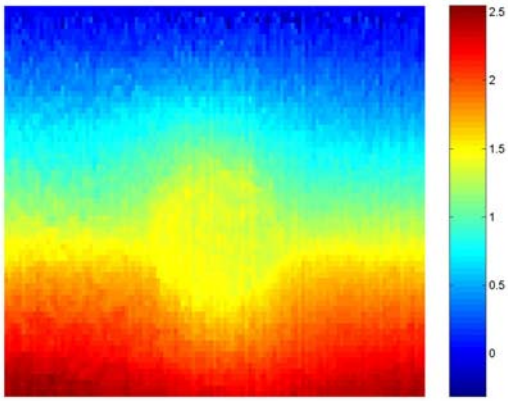

(a)

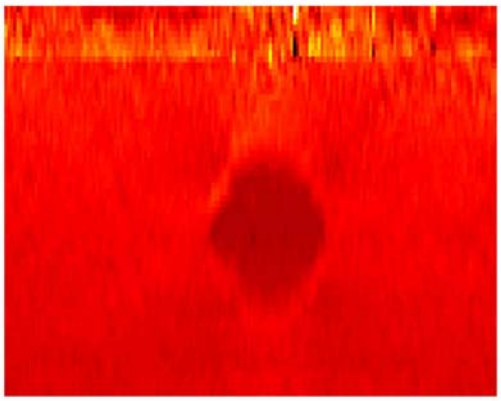

(b)

Fig. 6. Experimentally obtained displacement distribution (a) and the strain image (b)

Acknowledgments

This work was partially supported by Alexander von Humboldt-Foundation (Germany) through the Research Fellowship for Michael N. Rychagov at the Ruhr-University of Bochum, Department of Electrical Engineering.

Referenzen

[1] Gao, L., Parker, K.J., Lerner, R.M., Levinson, S.F. (1996) Imaging of the elastic properties of the tissue a review *Ultrasound Med. Biol.*, V. 22 (8), P. 959 - 977.

[2] Ophir, J., Garra, B., Kallel, F., Konofagou, E., Krouskop, T., Righetti, R., Varghese, T. (2000) Elastographic Imaging *Ultrasound Med. Biol.*, V. 26 (Suppl. 1), P. S23 – S29.

[3] Kroskoup, T.A., Vinson, S., Goode, B., Dougherty, D.A. (1987) A pulsed Doppler ultrasonic system for making noninvasive measurements of the mechanical properties of soft tissues *J. Rehab. Res. Dev.*, V. 24, P. 1 - 8.

[4] Parker, K.J., Huang, S.R., Musulin, R.A., Lerner, R.M. (1990) Tissue response to mechanical vibrations for sonoelasticity imaging *Ultrasound Med. Biol.*, V. 16, P. 241 - 246.

[5] Yamakoshi, Y., Sato, J., Sato, T. (1990) Ultrasonic imaging of internal vibration of soft tissue under forced vibration *IEEE Trans. Ultrason. Ferroelectron. Freq. Contr.* V. 37, P. 45 - 53.

[6] Catheline, S., Wu, F., Fink, M. (1999) A solution to diffraction biases in sonoelasticity: The acoustic impulse technique *J. Acoust. Soc. Am.*, V. 105 (5), P. 2941 – 2950.

[7] Sandrin, L., Tanter, M., Catheline, S., Fink, M. (2002) Shear modulus imaging with 2-D transient elastography *IEEE Trans. Ultrason. Ferroelectron. Freq. Contr*. V. 49 (4), P. 426 - 435.

[8] Ophir, J., Cespedes, I., Ponnekanti, H., Yazdi, Y., Li, X. (1991) Elastography: a quantitative method for imaging the elasticità of biological tissues *Ultrason. Imaging*, V. 13, P. 111 - 134.

[9] Srinivazan, S., Kallel, F., Souchon, R., Ophir, J. (2002) Analysis of an adaptive strain estimation technique in elastography *Ultrason. Imaging*, V. 24, P. 109 - 118.

[10] Hiltawsky, K.M., Krüger, M., Starke, C., Heuser, L., Ermert, H., Jensen, A. Freehand ultrasound elastography of breast lesions: clinical results. *Ultrasound Med. Biol.*, V. 27 (11), P. 1461 - 1469.

[11] Skovoroda, A.R., Emelianov, S.Y., Lubinski, M., Sarvazyan, A.P., O'Donnel, M., (1994) Theoretical analysis and verification of ultrasound displacement and strain imaging *IEEE Trans. Ultrason. Ferroelectron. Freq. Contr*. V. 41 (3), P. 302 - 313.

[12] O'Donnel, M., Skovoroda, A.R., Shparo, B.M., Emelianov, S.Y. (1994) Internal displacement and strain imaging using ultrasonic speckle tracking *IEEE Trans. Ultrason. Ferroelectron. Freq. Contr*. V. 41, P. 314 - 325.

[13] Skovoroda, A.R., Emelianov, S.Y., O'Donnel, M., (1995) Tissue elasticity reconstruction based on ultrasonic displacement and strain imaging *IEEE Trans. Ultrason. Ferroelectron. Freq. Contr*. V. 42 (4), P. 747 - 765.

[14] Sumi, C., Suzuki, A., Nakayama, K. (1995) Estimation of shear mudulus distribution in soft tissue from strain distribution *IEEE Trans. Biomed. Eng.* V. 42, P. 193 - 202.

[15] Kalel, F., Bertrand, M. (1996) Tissue elasticity reconstruction using linear perturbation method *IEEE Trans. Med. Imag.* V. 15, P. 299 - 313.

[16] Doyley, M. M., Bamber, J. C., Shiina, T., Leach, M. O. (1996) Reconstruction of elasticity modulus distribution from envelope detected B-mode data *IEEE Int. Ultrasonics Symp. (San Antonio, Texas),* (Piscataway, NJ: IEEE), V. 2, P. 1611 – 1614.

[17] Doyley, M. M., Meaney, P. M., Bamber, J. C. (2000) Evaluation of an iterative reconstruction method for quantitative elastography *Phys. Med. Biol.,* V. 45, P. 1521 – 1540.

[18] Landau, L.D., Lifshitz, E.M. Theory of elasticity. Course of theoretical physics. Volume 7. Pergamon Press, 1975.

[19] Duck, A.F. Physical properties of tissue Academic Press, 1990.

[20] Krouskop, T.A., Wheeler, T.M., Kallel, F., Hall, T. (1998) The elastic moduli of breast and prostate tissues under compression *Ultrason. Imaging*, V. 20, P. 151 - 159.

[21] Pesavento, A., Perrey, C., Krueger, M., Ermert, H. (1999) A time efficient and accurate strain estimation concept for ultrasonic elastography using iterative phase zero estimation *IEEE Trans. Ultrason. Ferroelect. Frequency Contr.*, V. 46 (5), P. 1057-1067.